



Searching for Low-redshift Faint Galaxies with MMT/Hectospec

Cheng Cheng^{1,2,11}, Jia-Sheng Huang¹, Christopher N. A. Willmer³, Hong-Xin Zhang^{4,5}, Matthew L. N. Ashby⁶, Hai Xu¹, Marcin Sawicki⁷, Stephane Arnouts⁸, Stephen Gwyn⁹, Guillaume Desprez¹⁰, Jean Coupon¹⁰, Anneya Golob⁷, Piaoran Liang¹, Tianwen Cao¹, Yaru Shi¹, Gaoxiang Jin¹, Chuan He¹, Shumei Wu¹, Zijian Li¹, Y. Sophia Dai¹, C. Kevin Xu¹, Xu Shao¹, and Marat Musin¹

¹ Chinese Academy of Sciences South America Center for Astronomy, National Astronomical Observatories, CAS, Beijing 100101, People's Republic of China
chengcheng@nao.cas.cn

² CAS Key Laboratory of Optical Astronomy, National Astronomical Observatories, Chinese Academy of Sciences, Beijing 100101, People's Republic of China
³ Steward Observatory, University of Arizona, 933 N. Cherry Avenue, Tucson, AZ 85721, USA

⁴ CAS Key Laboratory for Research in Galaxies and Cosmology, Department of Astronomy, University of Science and Technology of China, Hefei, Anhui 230026, People's Republic of China

⁵ School of Astronomy and Space Science, University of Science and Technology of China, Hefei 230026, People's Republic of China

⁶ Center for Astrophysics | Harvard and Smithsonian, 60 Garden Street, Cambridge, MA 02138, USA

⁷ Institute for Computational Astrophysics and Department of Astronomy and Physics, Saint Mary's University, 923 Robie Street, Halifax, Nova Scotia, B3H 3C3, Canada

⁸ Aix Marseille Université, CNRS, Laboratoire d'Astrophysique de Marseille, UMR 7326, F-13388 Marseille, France

⁹ Canadian Astronomy Data Centre, NRC-Herzberg, 5071 West Saanich Road, Victoria, British Columbia, V9E 2E7, Canada

¹⁰ Department of Astronomy, University of Geneva, ch. d'Écogia 16, CH-1290 Versoix, Switzerland

Received 2021 May 29; revised 2021 July 14; accepted 2021 July 24; published 2021 August 31

Abstract

We present redshifts for 2753 low-redshift galaxies between $0.03 \lesssim z_{\text{spec}} \lesssim 0.5$ with $18 \leq r \leq 22$ obtained with Hectospec at the Multi-Mirror Telescope. The observations targeted the XMM-LSS, ELAIS-N1 and DEEP2-3 fields, each of which covers $\sim 1 \text{ deg}^2$. These fields are also part of the recently completed Canada–France–Hawaii Telescope Large Area *U*-band Deep Survey and ongoing Hyper Suprime-Cam deep fields surveys. The efficiency of our technique for selecting low-redshift galaxies is confirmed by the redshift distribution of our sources. In addition to redshifts, these high signal-to-noise ratio spectra are used to measure ages, metallicities, and nuclear activity levels. In combination with the photometric catalog in *u*, *g*, *r*, *i*, *z*, *y* down to 27 AB mag, we are able to study the galaxy population down to stellar masses of $\sim 10^8 M_\odot$. This paper presents the observational strategy, the reduction procedure and properties of the galaxy sample. (The catalog can be accessed through the survey's website at http://mips.as.arizona.edu/~cnaw/Faint_Low_z/.)

Unified Astronomy Thesaurus concepts: Redshift surveys (1378); Post-starburst galaxies (2176); Galaxy formation (595); Quenched galaxies (2016); Dwarf galaxies (416); Spectroscopy (1558)

Supporting material: machine-readable table

1. Introduction

Galaxy populations are bimodally distributed in color, morphology, metallicity, and so on, which indicates a divergence in the galaxy evolution path (Takamiya et al. 1995; Baldry et al. 2004). The observational evidence indicates that galaxies evolve from the blue cloud to the red sequence (e.g., Faber et al. 2007). For bright galaxies, the blue and red populations can be defined well, however whether the bimodality relation can be extended to the faint end is still unclear.

Current surveys such as the Hyper Suprime-Cam Subaru Strategic Program (HSC-SSP; Aihara et al. 2018a, 2018b, 2019) and the Canada–France–Hawaii Telescope (CFHT) Large Area *U*-band Deep Survey (CLAUDS; Sawicki et al. 2019) provide catalogs that simultaneously cover large areas and reach faint magnitude limits. The finished CLAUDS project on the XMM-Newton Large-Scale Structure (XMM-LSS; Pierre et al. 2007) field, the European Large Area ISO Survey N1 area (ELAIS-N1;

Rowan-Robinson et al. 2004), the Deep Extragalactic Evolutionary Probe 2, Field 3 (DEEP2-F3; Newman et al. 2013), and the Cosmic Evolution Survey (COSMOS; Scoville et al. 2007) produce *u*-band catalogs of about 20 deg^2 and that are deep to 27 AB mag, which is about 2 mag deeper than previous large-area surveys like the CFHT Legacy Survey (CFHTLS; Cuillandre et al. 2012). The CLAUDS area is also covered by the HSC deep survey project with *u*, *g*, *r*, *i*, *z*, *y* bands at a depth of 27 AB mag. The matched CLAUDS+HSC catalog provides us with an unprecedented chance to study the faint galaxies statistically.

Almost all of our current understanding of galaxy formation and evolution, such as the bimodality of the color of galaxies, the luminosity, or stellar-mass functions, require accurate spectroscopic redshift (*spec-z*) measurements. Thus spectroscopic redshift surveys are the key to understanding the formation and evolution of galaxies. The advantage of the current wide-field deep survey is that we will have both a large sample with bright luminosities at high redshift and a large faint-galaxy sample at lower redshift.

Obtaining statistically significant samples of low-luminosity galaxies is rather difficult. Because of their faintness, the number of spectroscopically observed dwarf galaxies is very small even in large surveys like the Sloan Digital Sky Survey (SDSS; York et al. 2000; Strauss et al. 2002; Gunn et al. 2006)

¹¹ Corresponding author.

or Galaxy and Mass Assembly (GAMA; Driver et al. 2011). This is particularly true for galaxies in the red sequence. Deep-field imaging surveys (such as Ilbert et al. 2010 and Huang et al. 2013) suggest that there is a deficit of red galaxies at the low-mass end. This bias becomes more important in optical surveys with bright limiting magnitudes. To have a complete census of the low-mass galaxy population, we need to have redshifts of these faint galaxies.

Constructing a large faint-galaxy sample requires a redshift survey that combines a large area coverage with a deep magnitude limit. However, one dilemma of the spec- z survey is the difficulty of getting a large areal coverage and reaching very faint magnitudes simultaneously. SDSS is the most extensive spec- z survey and has covered 3600 deg² and reached the spec- z complete depth at $r \sim 17.7$ mag. The GAMA spec- z survey reaches a depth of $r \sim 19.8$ AB mag, and is complete in stellar masses to $\sim 10^9 M_\odot$. Nevertheless, the spectra of intrinsically very faint galaxies are often too noisy to be identified with high confidence or are biased toward containing predominantly emission-line galaxies, so surveys such as GAMA could be biased toward overrepresenting emission-line galaxies, and miss the low-redshift faint red galaxy population at $10^9 M_\odot$.

On the other hand, photometric redshifts for faint blue galaxies at lower redshifts suffer very large uncertainties due to their faintness and flat spectral energy distribution (SED) shape (Dahlen et al. 2013). Moreover, to obtain a reliable photometry redshift (phot- z) estimation, we also need a spec- z sample with a similar magnitude limit to estimate the accuracy of the phot- z results. Artificial intelligence (AI) shows great promise in obtaining the phot- zs with unprecedented accuracy and efficiency (Tanaka et al. 2018). However, AI also requires a large training sample with spec- z containing a variety of galaxy populations and brightnesses. Therefore, although we can estimate the redshift from the photometric catalogs, we still need spec- z to calibrate or train the phot- z results.

Nevertheless, because of constraints imposed by the efficiency of spectroscopic observations, spec- z survey projects are biased in the sense of containing mainly intrinsically bright objects. For the four CLAUDS fields, only the COSMOS field has the spec- z survey projects (e.g., zCOSMOS; Lilly et al. 2007, 2009) for both low- and high-redshift galaxies with a depth about $i \sim 22.5$ AB (also see Damjanov et al. 2018), and the XMM-LSS field has been covered by the VIMOS VLT deep survey (VVDS; Le Fèvre et al. 2005) to about $i \sim 24$ with low spectral resolution (Le Fèvre et al. 2013). The DEEP2-3 field is covered by the DEEP2 survey (Newman et al. 2013), which only focuses on the $z_{\text{spec}} > 0.5$ galaxies. The ELAIS-N1 field was selected from the SIRTF Wide-Area Infrared Extragalactic Survey (SWIRE; Lonsdale et al. 2003), and is mainly covered by SDSS DR13 for the bright targets (Lacy et al. 2013; Rowan-Robinson et al. 2013; Shirley et al. 2021). Thus, the CLAUDS fields still lack dense spectroscopic coverage for fainter targets.

To investigate the galaxy properties for the low-redshift¹² low-mass galaxies (e.g., $M_* \sim 10^{8.5} M_\odot$), we need a complete sample down to $r \simeq 22$ AB mag.¹³ The existing spectroscopic redshift surveys, such as SDSS, zCOSMOS, or the VIMOS

Ultra-Deep Survey (Le Fèvre et al. 2015), are either shallow with large areas, or deep enough within a small area. Previous low-mass galaxy spectroscopic redshift surveys such as the Metal Abundances across Cosmic Time Survey (Ly et al. 2016a, 2016b; Shin et al. 2021) only focused on the emission-line galaxies, which would bias to young, star-forming galaxies. The ongoing spec- z survey projects such as the Dark Energy Spectroscopic Instrument (DESI Collaboration et al. 2016), Subaru Prime Focus Spectrograph (Tamura et al. 2016) and Hobby-Eberly Telescope Dark Energy Experiment (Hill et al. 2008) plan to cover large areas with much deeper survey depth, but these survey projects are very time consuming or are only under initiation. Therefore, we propose a new redshift survey for the low-redshift faint galaxies based on the CLAUDS+HSC catalog with MMT/Hectospec.

MMT/Hectospec (Fabricant et al. 2005) is a multifiber spectrograph that can obtain 300 fiber spectra simultaneously within 1° diameter, and thus is very efficient for redshift surveys. Moreover, for the low-redshift galaxies, the moderate resolution spectrum (resolution power about 2700) covering from 3600–8900 Å will reveal most of the optical spectrum lines such as [O II], Ca II, H β , [O III], Mg b, Na D, H α , [N II], and [S II], which are not only helpful in identifying the redshift, but also necessary to characterize the physical properties such as star formation rate, metallicity, galactic activity, etc.

To study the galaxy population, especially the low-redshift faint-field galaxies, we performed a redshift survey in the HSC survey deep fields by MMT/Hectospec. Previous low-redshift redshift surveys such as Satellites Around Galactic Analogs (Geha et al. 2017; Mao et al. 2021) and the Southern Stellar Stream Spectroscopic Survey (Li et al. 2019) focused on the satellite galaxies and stellar streams at $z_{\text{spec}} \lesssim 0.02$, the properties of which would be affected by the environment. There are very few local bright galaxies ($z_{\text{spec}} < 0.02$) in the HSC deep fields, because the deep fields are selected to study the galaxies at high redshift, thus we can expect that the redshift survey in the HSC deep fields can provide us the low-redshift faint-field galaxies at $z_{\text{spec}} \gtrsim 0.02$. HSC+CLAUDS provides us with a photometric catalog reaching 27 AB mag, which is faint enough for us to select low-redshift faint-galaxy candidates, and the MMT 6.5 m mirror can push the redshift survey depth to about $r = 22$ AB mag, which roughly corresponds to stellar masses of $10^{8.5} M_\odot$ at redshift 0.15. This sample reaches about 4 mag deeper than SDSS, and 2 mag deeper than the GAMA survey, which will be critically important to understanding the faint-galaxy properties and the calibration of the phot- z to spec- z to the faint end.

In this paper, we describe our survey strategy, redshift catalogs and preliminary results of this survey. We arrange this paper as follows: Section 2 describes the target selection procedure, the MMT/Hectospec observations and the data reduction method. In Section 3, we show the typical spectrum examples as well as the first look results. We close with a summary in Section 4.

2. Observations and Data Reduction

2.1. Target Selection

The low-redshift galaxy population with stellar mass $\sim 10^8 M_\odot$ should have $r \sim 22$ at $z_{\text{spec}} \simeq 0.15$, thus we select the galaxies with $r < 22$. The four CLAUDS fields are covered by SDSS, thus the galaxies with $r < 17.7$ have complete spec- z . So we limit our

¹² In this paper, we refer the galaxies at $0.03 < z_{\text{spec}} < 0.5$ as low-redshift galaxies, and the galaxies at $z_{\text{spec}} < 0.03$ as local galaxies.

¹³ Galaxy stellar mass about $M_* \sim 10^{8.5} M_\odot$ corresponds to about $M_r \simeq -17$ AB mag, which is about r -band 22 AB mag at redshift 0.15 (Mahajan et al. 2018).

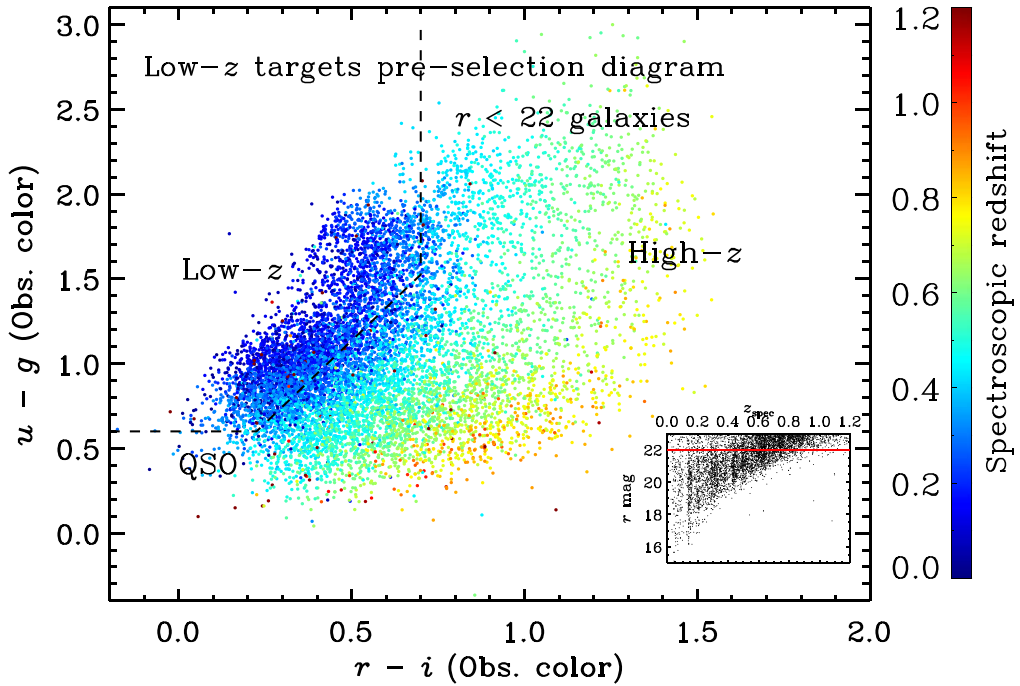


Figure 1. The low- z target preselection method. We show data from the XMM-LSS field as an example. The color code represents redshifts from prior surveys including SDSS, VVDS (Le Fèvre et al. 2005), the VIMOS Public Extragalactic Survey (VIPES; Mohammad et al. 2018), PRIm Multi-object Survey (PRIMUS, Coil et al. 2011), and eBoss (Dawson et al. 2016). From the main plot, we can see a clear trend that redshifts change with color. We remove the blue QSOs in the lower-left corner by setting $u - g > 0.6$. Our selection criteria ($u - g > 0.6$; $r - i < 0.7$; $u - g > 1.95 \times (r - i) + 0.16$) are shown by the dashed lines, which select most of the galaxies at $z_{\text{spec}} < 0.35$. The inset in the lower right shows the distribution of the r -band magnitude and redshift. The red line shows the $r = 22$ limit, which enables us to remove the contamination from the high- z galaxies.

targets to $18 < r < 22$. When the observations were initiated, the CLAUDS survey was essentially complete, with full coverage in XMM-LSS and ELAIS-N1, while HSC data were not yet fully released. Since the r -band 22 mag is still above the limit magnitude of the previous survey projects, we selected our targets from the CFHTLS catalog (Gwyn 2012) for the CLAUDS-XMMLSS field, from the ELAIS-N1 catalog (González-Solares et al. 2011) for the CLAUDS-ELAIS-N1 field, and from the Stripe-82 catalog (Jiang et al. 2014) for the CLAUDS-DEEP23 field. The minor differences between the photometric passband definitions will not affect our target selection.

To target specifically galaxies at lower redshifts, we adopt a color–color cut, similar to the method used in the DEEP2 project (Newman et al. 2013) to preselect our targets. Figure 1 illustrates the selection methods. Galaxies with $z_{\text{spec}} < 0.35$ are located in the upper left of the $u - g$, $r - i$, color–color diagram, and are separated into two groups, indicating a blue and red population in colors. The inset in Figure 1 shows the r -band magnitude and redshift distribution. So excluding galaxies fainter than $r = 22$ AB mag removes most higher-redshift galaxies. We select our sample galaxies by the criteria: $u - g > 0.6$; $r - i < 0.7$; $u - g > 1.95 \times (r - i) + 0.16$. The CLAUDS catalog is deep enough for us to select the $u - g$ red galaxies, which are candidate low-mass red galaxies. We select the upper-left corner of the dashed line selection criterion in Figure 1. We also remove the foreground stars by the CLASS_STAR flag, and the galaxies with previous spec- z measurements. The survey was designed to observe galaxies brighter than $r = 22.5$, which is the detection limit for galaxies in 1 hr integrations. Therefore, MMT/Hectospec is exactly the instrument suitable for this project.

We were allocated 6.5 MMT/Hectospec nights (4.5 dark nights and 2 gray nights) from the Telescope Access Program (TAP) to observe the XMM-LSS, ELAIS-N1, and DEEP2-3 fields (TAP2016B, ID:21; TAP2017A, ID: 27, TAP2017B, ID: 33. PI: Cheng Cheng). Hectospec is an optical fiber-fed spectrograph that can obtain 300 spectra at the same time in a 1 deg^2 field of view for one configuration. Figure 2 shows the location of our targets in the three CLAUDS fields. We chose the pointing positions that were covered by previous spec- z surveys to increase the survey completeness. Since the density of the $r \lesssim 22$ targets at low redshift is about 2000 per degree (Wirth et al. 2004), we chose only one pointing per field with several configurations. The observations are run in queue mode and the user provides a previously calculated configuration file containing the R.A. and decl. positions, magnitudes, and rank for each object, using the `xfitfibs`¹⁴ code developed by the Hectospec Instrument team (Roll et al. 1998). For each run, we assigned at least 40 fibers for the sky, 10 fibers for F-star flux calibrators and 3 fibers for the Guide stars. `xfitfibs` will assign the fiber by the rank and class of each target. To avoid fiber entanglement, some of the fibers may not be assigned to an object. So we also add some 8 μm detected sources from the SWIRE survey with low rank to make full use of the available fibers. `xfitfibs` calculates several configurations in a single field simultaneously in order to sample as many objects as possible in a given rank (i.e., priority). As each object is assigned to a fiber, it is “removed” from the catalog. To obtain longer exposures (i.e., over more than one configuration), some faint $u - g$ red sources were included more than once in the source catalog used by `xfitfibs`. But we found this method

¹⁴ <https://www.cfa.harvard.edu/mmti/hectospec/xfitfibs/>

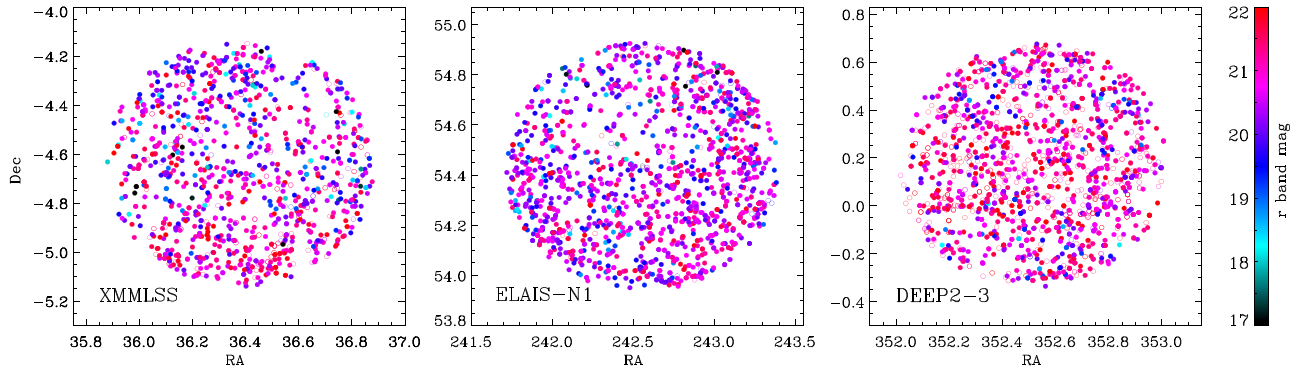


Figure 2. Survey region in XMM-LSS, ELAIS-N1, and DEEP2-3. We color the target position by the r -band magnitude. The filled circles show the targets with reliable redshifts ($q_z \geq 3$) while the open circles represent observed galaxies that did not provide a reliable redshift.

does not provide us with better signal-to-noise ratio (S/N) because of the low flux calibration accuracy and different weather in each night.

The observations were obtained in 2016 October for the XMM-LSS and DEEP2-3 fields (2.5 dark nights), 2017 April for ELAIS-N1 (2 dark nights), and 2017 October for the XMM-LSS and DEEP2-3 fields (2 gray nights). Due to the weather and instrument malfunction, we only succeeded in obtaining raw data for 20×1.5 hr exposure in total, which is about 4 nights' data.

2.2. MMT/Hectospec Data Reduction

The data are reduced by the HSRED2 pipeline,¹⁵ which will automatically perform the wavelength calibration, flux calibration, spectral extraction, etc., from the raw data, and produce the calibrated spectra. The flux is calibrated by the 10 F-star simultaneously obtained for each run. The final redshifts are identified by the spec2d pipeline¹⁶ used by the DEEP2 survey project, which measures redshifts using cross correlation with templates that contain absorption- and emission-line spectra. Three people then check the quality of the spec- z fitting result individually. When the fitted spec- z is not matched by the location of the spectral lines, we refit the spec- z to match the spectral lines within a smaller wavelength range. We assign the quality flag (q_z) of the spec- z with the same criterion as the DEEP2 survey (Willmer et al. 2006; Newman et al. 2013). Finally, we check the spec- z catalog from the three persons and find good consistency. For the targets with inconsistent spec- z results, their reliability will be changed from the average q_z estimated from the visual inspection to $q_z - 1$. Low- z galaxies have many observable emission- and absorption-line features in the observation window, thus the quality would be either identified by two clear lines, or there would be no available features to help the identification. So almost all galaxies in our sample have the quality flag 4, or an unreliable quality flag as 1 or 2.

In total, we obtained 6000 spectra, 2753 of which have a highly reliable quality ($q_z \geq 3$). The left panel of Figure 3 shows the observed color-magnitude diagram and the histogram of our full sample observed with MMT/Hectospec (in black) and the targets with $q_z \geq 3$ (in red). The redshift identification success rate is the ratio between the red and black histograms, respectively, which is about 50% for our sample

with r -band 22 mag, or $u - r \gtrsim 2.5$. Red targets usually have weak emission lines, thus it is more difficult to identify their redshift. Galaxies with low surface brightness in the fiber aperture are also challenging to obtain spectra with S/N high enough to identify the redshifts. The success rate is also related to the exposure time, weather, Moon phase, etc.

The right panel of Figure 3 shows the redshift distribution of galaxies with $q_z \geq 3$. (164 SWIRE targets have reliable spec- z at the range of $z_{\text{spec}} < 0.6$ in our survey. We do not treat the SWIRE targets separately in the following analyses.) Our targets are selected from $r < 22$, which is highly complete because the optical survey depth is about r -band 2527 mag, much deeper than $r = 22$. The observed-frame $u - g$, $r - i$ color-color selection aims to select the galaxies at $z_{\text{spec}} < 0.35$, however there is no clear division between the $z_{\text{spec}} > 0.35$ and $z_{\text{spec}} < 0.35$ galaxies in the color-color diagram, else there would be some low-redshift galaxies outside the selection box, or vice versa. Our results show that about 20% (553 out of 2753) of the galaxies in our selection box are at $z_{\text{spec}} > 0.35$, and if the redshift distribution of the targets close to the color-color lines is symmetric, we can expect an 80% completeness for the broadband color-color selection method. The redshift identification success rate also limits our sample completeness, especially for the faint or red galaxies. Based on the histograms in Figure 3, targets selected by the color-color diagram have a success rate about 80% for the galaxies $r < 21$ or observed-frame color $u - r < 2$, and only 50% for the galaxies about $21 < r < 22$ and observed-frame $u - r > 2.5$. The redshift distribution histogram also shows the presence of large-scale clustering structures at several redshift bins, which is also revealed in the inset of Figure 1. The catalog is listed in Table 1,¹⁷ and can be accessed through the web page of this survey.

We show all of our spectra with $q_z \geq 3$ in Figure 4 and denote the position of prominent lines. In addition to the emission lines, several prominent absorption lines can be identified such as $H\delta$, K , H , G -band, Mgb, and Na D. These lines are important in revealing the poststarburst features, age, outflows, and metallicity. We fit the emission lines by one Gaussian profile plus an n -order polynomial to model the continuum. We also measure the D_n4000 parameter (Balogh et al. 1999), which is sensitive to the stellar age. To reduce the uncertainty of the flux calibration, we estimate the metallicity by the $[\text{N II}]/\text{H}\alpha$ and the Baldwin–Phillips–Telervich (BPT) diagram (Baldwin et al. 1981) of $[\text{N II}]/\text{H}\alpha$ versus $[\text{O III}]/\text{H}\beta$

¹⁵ <http://mmt.org/~rcool/hsred/index.html>

¹⁶ <http://deep.ps.uci.edu/spec2d/>

¹⁷ http://mips.as.arizona.edu/~cnaw/Faint_Low_z/

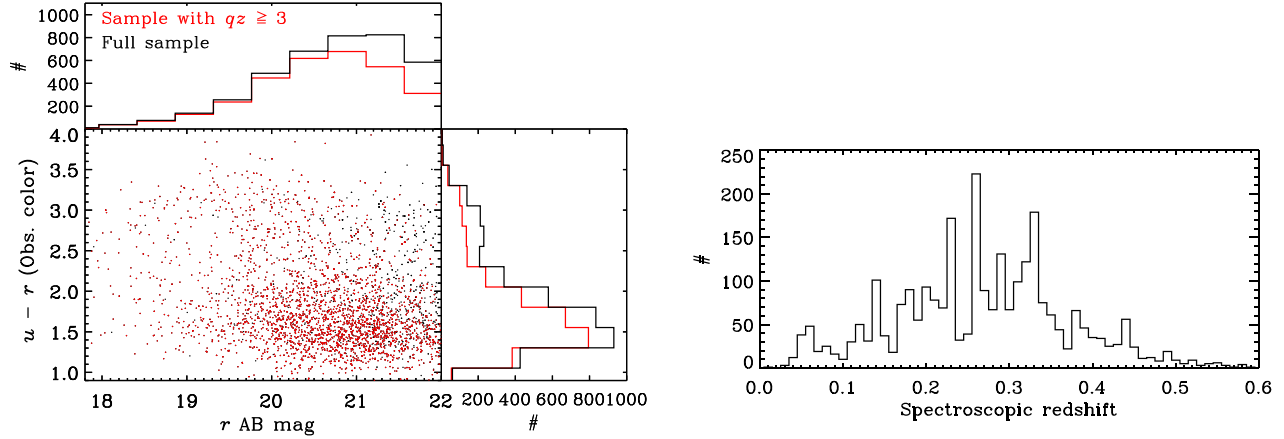


Figure 3. Left panel: observed color–magnitude diagram of our full sample observed by MMT/Hectospec. We highlight the galaxies with redshift quality $qz \geq 3$ in red. The spec- z identification rate is the ratio of the red and black histograms, which is about 50% for the galaxies about r -band 22 AB magnitude, or $u - r \gtrsim 2.5$. Right panel: the redshift distribution of our final results.

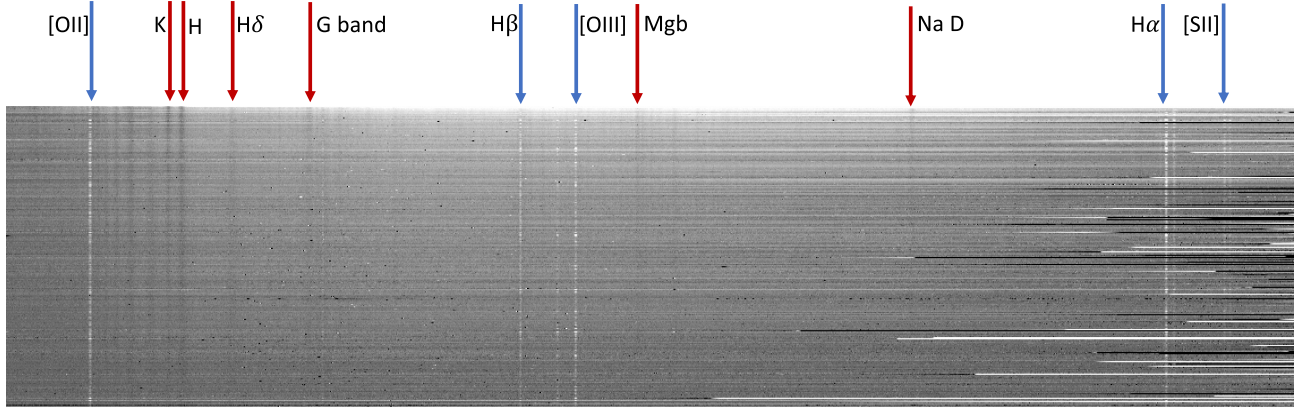


Figure 4. All one-dimensional galaxy MMT/Hectospec spectra for which reliable redshifts could be estimated, displayed in deredshifted two-dimensional format with major features noted.

Table 1
Redshift Catalog of Galaxies We Observed in the XMM-LSS, ELAIS-N1, and DEEP2-3 Fields

ID	R.A. (J2000)	Decl. (J2000)	$r_{\text{aper}} (1'')$	z_{spec}	qz
J022455.7-045217.2	36.23213053	-4.87143230	20.05	0.435135 ± 0.000083	4
J022404.9-044628.7	36.02022171	-4.77463340	20.62	0.069242 ± 0.000011	4
J022422.8-050130.2	36.09491587	-5.02506590	21.18	0.361262 ± 0.000150	3
J022415.1-044629.2	36.06300831	-4.77476690	20.39	0.313309 ± 0.000019	4
J022451.1-045053.0	36.21307254	-4.84805010	20.30	0.151206 ± 0.000017	4
J022438.4-043736.3	36.16017222	-4.62673950	19.99	0.151956 ± 0.000055	4
J022420.2-042341.3	36.08414054	-4.39479830	20.19	0.173245 ± 0.000010	4
J022448.3-042941.4	36.20107055	-4.49483250	21.28	0.361714 ± 0.000272	4
J022435.4-042743.1	36.14740133	-4.46197270	18.68	0.055294 ± 0.000029	4
J022340.9-043345.5	35.92041135	-4.56262590	18.16	0.115660 ± 0.000014	4
J022447.4-043555.9	36.19755864	-4.59885070	19.74	0.141267 ± 0.000037	4
J022549.7-041918.7	36.45696402	-4.32187180	19.64	0.318949 ± 0.000052	4
J022531.5-044045.5	36.38142228	-4.67929320	19.76	0.264473 ± 0.000064	4
J022540.5-042736.0	36.41873002	-4.45999770	19.97	0.311829 ± 0.000042	4
J022505.3-042214.4	36.27206683	-4.37067170	21.10	0.364456 ± 0.000066	4
J022550.1-041050.7	36.45874500	-4.18075320	15.66	0.043963 ± 0.000032	4
J022542.8-041650.0	36.42831087	-4.28054860	21.32	0.138524 ± 0.000070	4
J022544.7-041142.8	36.43630028	-4.19522290	20.28	0.287854 ± 0.000034	4
J022509.2-044359.3	36.28851414	-4.73312850	21.53	0.279311 ± 0.000054	4

(This table is available in its entirety in machine-readable form.)

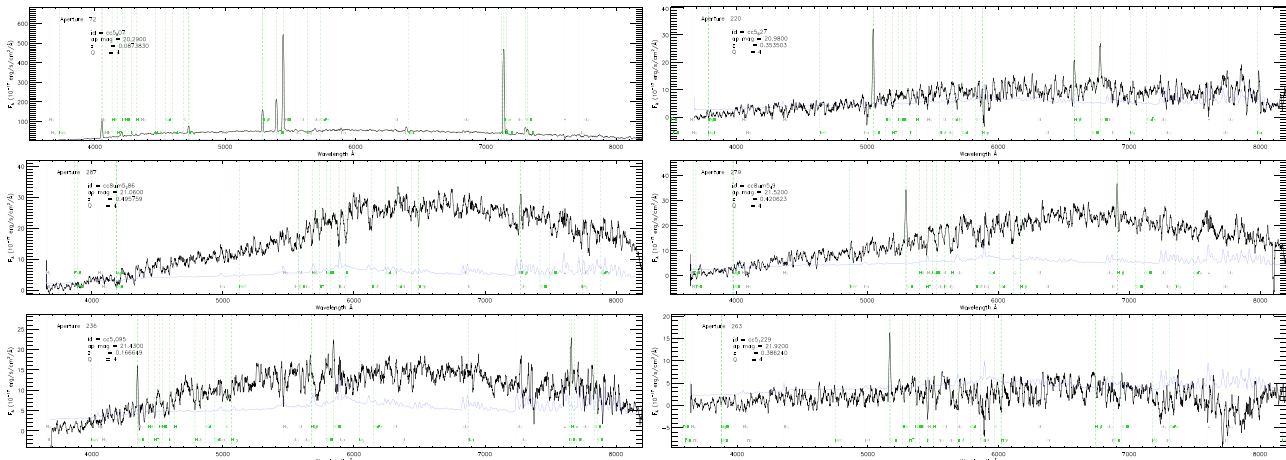


Figure 5. Examples of MMT/Hectospec spectra. The r -band magnitudes increase from top to bottom. The green dashed lines show the emission- or absorption-line positions. The black lines are the galaxy spectra, while the blue lines are the inverse $\sqrt{\text{variance}}$ spectra. We denote the target name, r -band aperture magnitude within $1''$, identified redshift, and the redshift quality (qz) in each panel. Redshifts for galaxies brighter than $r = 21$ can be identified clearly. For the galaxies fainter than $r = 21$, the redshift of galaxies with bright emission lines can be identified. The bottom panel shows no clear continuum due to the faintness, while the emission lines still help us to measure the redshift.

so that the flux ratio always comes from two emission lines at close wavelengths.

2.3. Spectra Examples

We show some examples of our MMT/Hectospec spectra in Figure 5. The r -band magnitude on each side increases from the top to the bottom panel. For 1.5 hr exposure time, the S/N of the MMT/Hectospec spectra are high enough to identify the emission and absorption lines for the galaxies brighter than $r = 21$ AB mag, and bright enough to identify emission lines for $21 < r < 22$. For the faint emission-line galaxies, we can only identify the redshifts and cannot have reliable D_n4000 measurements. The flux calibration from F-star can normalize the continuum flux, but does not calibrate the shape of the continuum very well. The data from the two gray nights in 2017B are affected by moonlight, so we can only get a reliable redshift.

2.4. Multiwavelength SED Fitting

The survey fields have been covered by CLAUDS in the u band, HSC in the g , r , i , z , y bands, and also covered by the near-infrared (NIR) images from the VISTA Deep Extragalactic Observations survey (Jarvis et al. 2013) in the XMM-LSS field, the UKIRT Infrared Deep Sky Survey/Deep Extragalactic Survey (Lawrence et al. 2007) in the ELAIS-N1 field and the VISTA-CFHT Stripe 82 Survey (Geach et al. 2017) in the DEEP2-3 field. We match our redshift catalog to the CLAUDS and HSC DR2 catalogs, which have much deeper limiting magnitude (~ 27), and more reliable photometry. Some of our targets have bright neighboring stars in the HSC catalog, which were flagged or not contained in the HSC catalogs. For these objects, we use the photometry from the target selection catalogs, which have brighter saturation magnitudes than the HSC survey, and are much less affected by the bright stars. We also match our catalog to the archive UKIRT J - and K_s -band catalogs to have better coverage in the NIR bands in the final multiwavelength catalog.

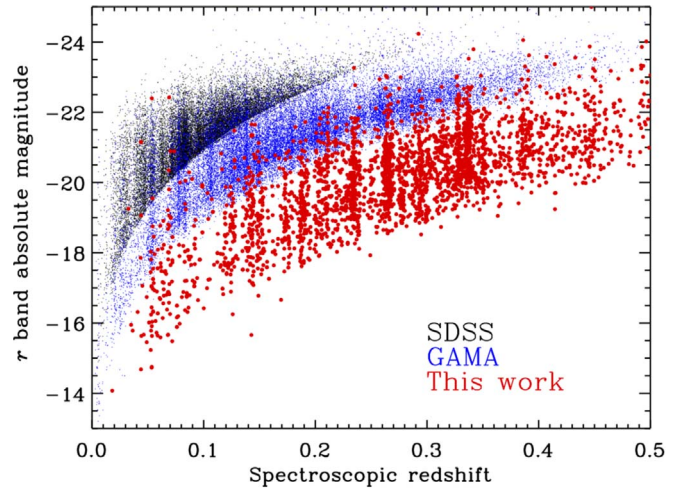


Figure 6. Redshift and absolute magnitude plot of this spectroscopic redshift survey compared to the SDSS and GAMA surveys. At the same redshift, our survey is about 2 mag deeper than the previous surveys. For the galaxies at about $M_r \simeq -18$, the SDSS and GAMA sample only have the galaxies at $z_{\text{spec}} < 0.05$, while our results have the galaxies at $z_{\text{spec}} < 0.2$, where peculiar motions can be neglected.

We derive the absolute magnitude by the definition of $m_R = M_Q + DM + K_{QR}$ (Hogg et al. 2002), where m_R is the observed magnitude in band R , M_Q is the absolute magnitude in band Q in the emitted frame, DM is the distance modulus and the K_{QR} is the K -correction factor between the observed R band and the rest-frame Q band. The K -correction factor of the absolute magnitude of our sample is derived by the Coleman et al. (1980) and Kinney et al. (1996) template spectra with the K -correction formulae given by Hogg et al. (2002). We show the results in Figure 6 and compare with the previous low-redshift spec- z survey results from SDSS and GAMA. We select 20,000 SDSS sources with random R.A. and decl. and the full GAMA catalog (Driver et al. 2011, 2016) in the G09, G12, and G15 fields as a comparison sample. Within the same redshift range, our results reach about 2 mag fainter than the previous works. Galaxies in our sample with $M_r \simeq -18$ are

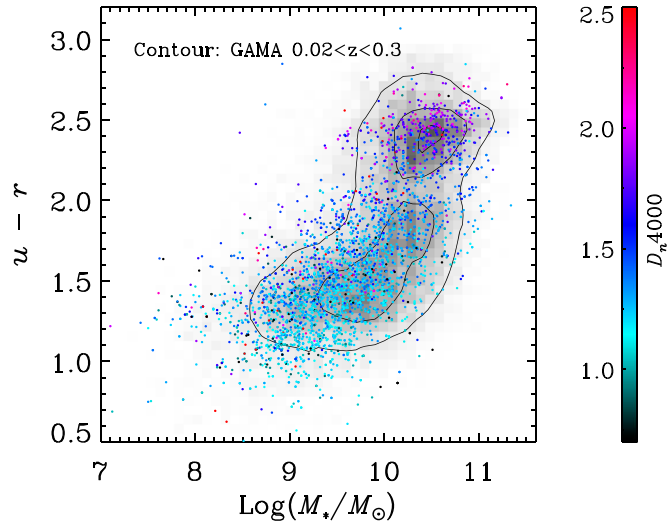


Figure 7. Color-magnitude and color-stellar mass plots. We compare with the GAMA sample at $0.02 < z_{\text{spec}} < 0.3$. We color our results with the D_n4000 value.

located at $z_{\text{spec}} \sim 0.1$, a distance where peculiar motions can be neglected. Nevertheless, the SDSS and GAMA surveys mainly sample galaxies with $M_r \simeq -18$ at redshifts $z < 0.05$. Therefore, our sample reaches lower stellar masses than the previous surveys at higher redshift.

We fit the SED by `fastpp`¹⁸ (Kriek et al. 2009) using the broadband photometry and our spec-zs to measure the stellar mass. We adopt the Bruzual & Charlot (2003) stellar population synthesis models, Chabrier initial mass function (Chabrier 2003), and the Calzetti et al. (2000) dust extinction law with the attenuation in the range of $0 < A_v < 3$. Figure 7 shows the absolute $u - r$ color and stellar-mass diagram. We also show the contours of the color-mass diagram of GAMA of the galaxies at $0.02 < z_{\text{spec}} < 0.3$. Our results are consistent with GAMA, while the stellar masses are a bit lower than GAMA.

3. Results

3.1. Emission-line Diagnosis

The BPT diagram is widely used to identify the emission-line ionization source based on the line ratios (Baldwin et al. 1981; Kewley et al. 2006). We show the BPT diagram in Figure 8 where the colors represent different stellar-mass ranges. We also show the result from SDSS to show the typical values of the low- z galaxies. Nearly all the galaxies in our sample are star-forming galaxies. Gas-phase metallicities can be derived from the strong line ratios (Kewley & Ellison 2008; Maiolino & Mannucci 2019). We denote the metallicity that is derived from $[\text{N II}]/\text{H}\alpha$ (Curti et al. 2020) in the upper x -axis. The mass-metallicity trend (Tremonti et al. 2004) can also be seen in our sample, where the low-metallicity targets have stellar masses of $\sim 10^8 M_\odot$.

3.2. Rest-frame U-V versus V-I Diagram

The UVJ diagram (rest-frame $U-V$ versus rest-frame $V-I$) has been widely applied to help constrain galaxy properties because extinction and age vary in orthogonal directions

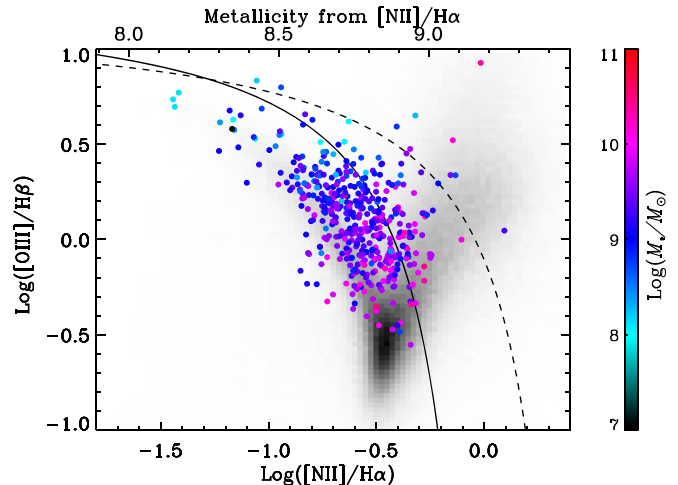


Figure 8. BPT diagram of our sample with emission lines. The gray scale shows the distribution of SDSS galaxies. We also plot the Kauffmann and Kewley lines (Kewley et al. 2001; Kauffmann et al. 2003), which classify galaxies as being mainly ionized by active galactic nucleus or star formation. The upper horizontal axis show the metallicity that derived from the $[\text{N II}]/\text{H}\alpha$ (Curti et al. 2020).

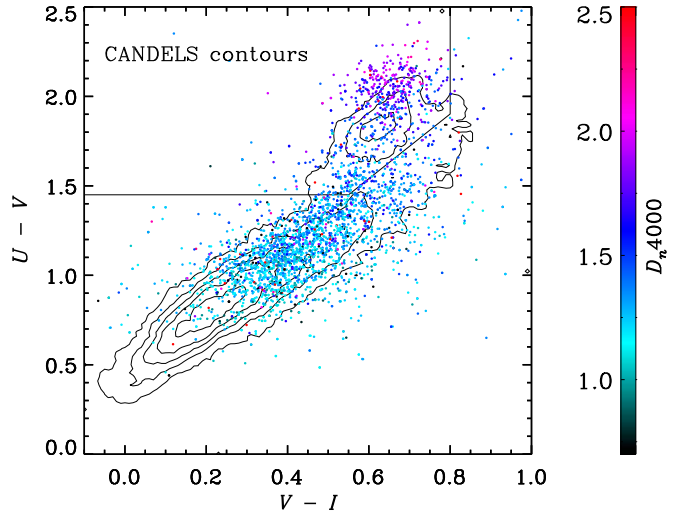


Figure 9. The $U - V$ vs. $V - I$ diagram of our sample overplotted on the contours of CANDELS UVI results. The solid line separates the quiescent galaxy population (upper left) from the dusty (upper right) and star-forming (lower left) galaxy populations. We use the galaxy sample from the CANDELS catalog with $z_{\text{phot}} < 1$.

(Labbé et al. 2005; Williams et al. 2010; Fang et al. 2018; Leja et al. 2019). However, because of the limited NIR coverage of our sample, we followed Wang et al. (2017) and Liu et al. (2018) by using the UVI distribution (rest-frame $U-V$ versus $V-I$, Figure 9) to separate dusty from old populations. We define the old population region based on the quiescent galaxies selected from the UVJ diagram. Our result shows a similar distribution as the the $z_{\text{phot}} < 1$ sample from the Cosmic Assembly Near-infrared Deep Extragalactic Legacy Survey (CANDELS, Grogin et al. 2011; Koekemoer et al. 2011), which is denoted by the contours.

3.3. Absorption-line Galaxies: Quenching of the Low-mass Galaxies

Quenching of low-mass galaxies is commonly studied in galaxy clusters (Toloba et al. 2014; Roediger et al. 2017;

¹⁸ <https://github.com/cscreib/fastpp>

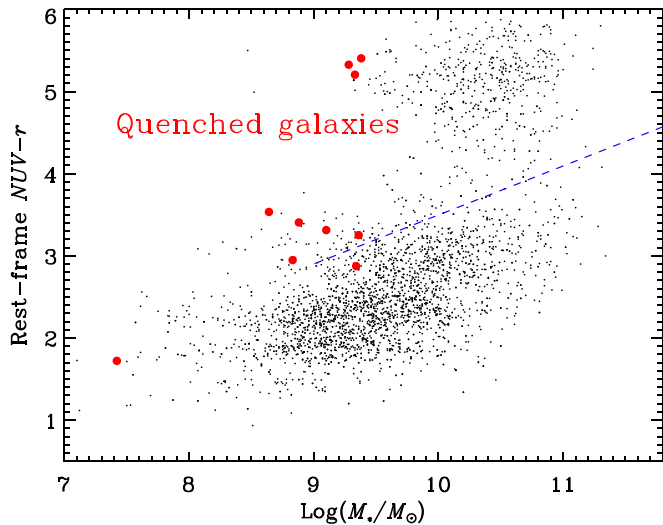


Figure 10. NUV – r vs. stellar mass diagram of our sample. The blue dashed line represents the criterion from Pan et al. (2016) to separate red from star-forming galaxies. This line is generated from the SDSS data with stellar mass lower to $10^9 M_\odot$. The red filled circles are the low-mass galaxies ($M_* < 10^{9.5} M_\odot$) with no clear emission line, which are the quenched galaxies we found in this spec- z survey.

Danieli et al. 2018), where the massive galaxies reduce the gas supply to dwarf galaxies by ram pressure, tidal interactions, or other mechanisms (Simon 2019). Figure 8 shows that most of our galaxies are star-forming galaxies at $\sim 10^9 M_*/M_\odot$, so we can use our sample to understand the quenching features of field galaxies at $\sim 10^9 M_*/M_\odot$.

On the other hand, previous studies show that the fraction of isolated quenching galaxies in the field is extremely small at the low-mass end ($10^7 < M_*/M_\odot < 10^9$, or, $-18 < M_r < -12$) (Geha et al. 2012). In this case, the low-mass galaxies should either sustain the current star formation, grow into massive galaxies, or be merged into nearby massive galaxies. However, star formation history analyses of the ultrafaint local dwarf galaxies (Brown et al. 2014) show that 80% of stars were formed at about $z \sim 6$ and 100% of stars were formed at $z \sim 2$. Therefore, we could expect to find the low-mass quenched galaxies at low redshift.

The quenching and star-forming galaxy population can be shown clearly in the rest-frame NUV – r versus stellar mass diagram (Salim et al. 2005; Salim 2014; Pan et al. 2016), where the rest-frame NUV flux is proportional to the star formation rate, therefore the NUV – r roughly represents the specific star formation rate. One of the advantages of the NUV – r diagram is the clear separation between the galaxy populations (Salim 2014). Figure 10 shows the NUV – r versus mass of our sample, where we can see a clear separation between the blue and red population, and the green valley where the galaxies might be poststarburst galaxies.

We searched for the presence of strong Balmer absorption and weak or no emission-line flux in the spectra of all galaxies with $\log(M_*/M_\odot) < 9.5$. We find 10 galaxies with no clear emission lines ($S/N < 3$) and these are shown in Figure 11 for $\log(M_*/M_\odot) < 9$, Figure 12 for $9 < \log(M_*/M_\odot) < 9.5$, and in Figure 10 with red dots. The very weak emission lines, the strong H δ (if detected) and the H , K lines of the spectrum

indicate a lack of ionized gas and that they are quenched from the starburst phase and may evolve into the red population. We show the star-forming galaxy separation criteria from Pan et al. (2016), where they only consider the galaxy sample with a stellar mass larger than $10^9 M_\odot$ as a reference. The NUV – r color of these galaxies shows that the 10 weak emission-line galaxies are above the main sequence of the star-forming galaxies in Figure 10, more likely in the green valley. We observed the absorption-line galaxy with the lowest stellar mass in Figure 10 by using the Hale telescope/DBSP (TAP2017B, ID: 01, PI: Cheng Cheng) confirming the 0.036 spectroscopic redshift of this galaxy, and find no evidence of emission lines. We also confirmed that there is no nearby galaxy within 50 kpc brighter than this target. Geha et al. (2012) have shown that the isolated low-mass quenched galaxies are rare. A detailed study of these low-mass absorption-line galaxies, such as whether they are isolated galaxies, will be presented in a forthcoming paper.

We also take advantage of our accurate phot- z to study the low-mass quenching population. The ongoing and upcoming multiwavelength deep survey projects such as HSC and the Vera C. Rubin Observatory’s Legacy Survey of Space and Time (LSST Science Collaboration et al. 2009) data will produce a vast sample of high-quality photometry catalogs. Meanwhile, phot- z techniques such as machine learning and empirical template fitting, as well as the hybridization of several methods (Salvato et al. 2019) can provide accuracies of 2% or even better (Tanaka et al. 2018; Zhou et al. 2019; Nishizawa et al. 2020; Schmidt et al. 2020), which can be used to enlarge the sample of low-redshift low-mass passive galaxies for follow-up spectroscopic identification. We compare the phot- z results of our sample from the CLAUDS + HSC dr2 SEDs (G. Desprez et al. 2021, in preparation) and our spec- z results in Figure 13. The phot- z of our sample can recover the spec- z very well with a scatter σ_{NMAD} about 2.3% and a redshift offset about 0.006. The large-scale clustering structures shown in z_{spec} (see also Figure 3, right panel) are not recovered in the phot- z results, implying the limitation of studying the cosmological large-scale structure with phot- z data (also see Sohn et al. 2021). In the forthcoming work, we will study the low-mass red galaxies based on the spec- z and the phot- z to explore the quenching process in the low-mass galaxies.

4. Summary

We select a sample of $0.03 \lesssim z_{\text{spec}} \lesssim 0.5$ and carry out a spectroscopic redshift survey using MMT/Hectospec. The redshift distribution validates our target selection method, and we acquired spectra for 2753 galaxies. In this paper, we release the spec- z catalog including R.A., decl., spec- z , and qz . We demonstrate that our selection method is effective at identifying low-mass quenched galaxies. The spec- z catalog was used to calibrate the phot- z s in three surveyed fields, expanding the sample of low-mass galaxies. These combined (spectroscopic and photometric redshift) catalogs are being used to analyze the population of low-mass field galaxies, which are the subject of a forthcoming paper.

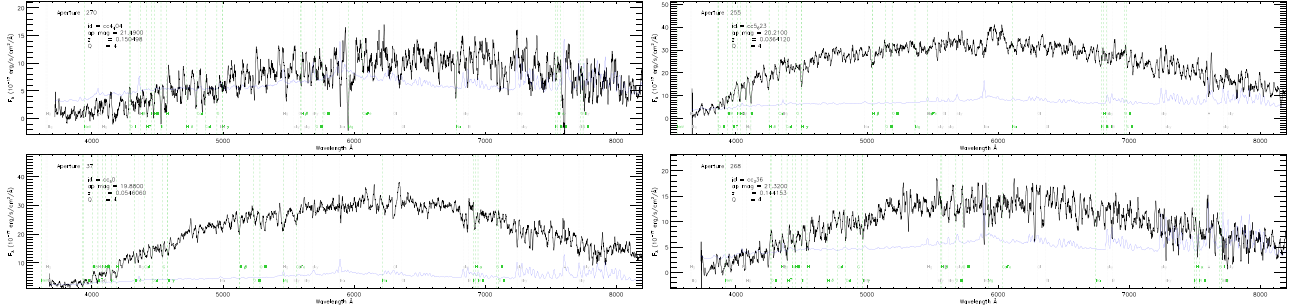


Figure 11. Example of spectra of low-mass galaxies ($M_* < 10^9 M_\odot$) with weak emission lines.

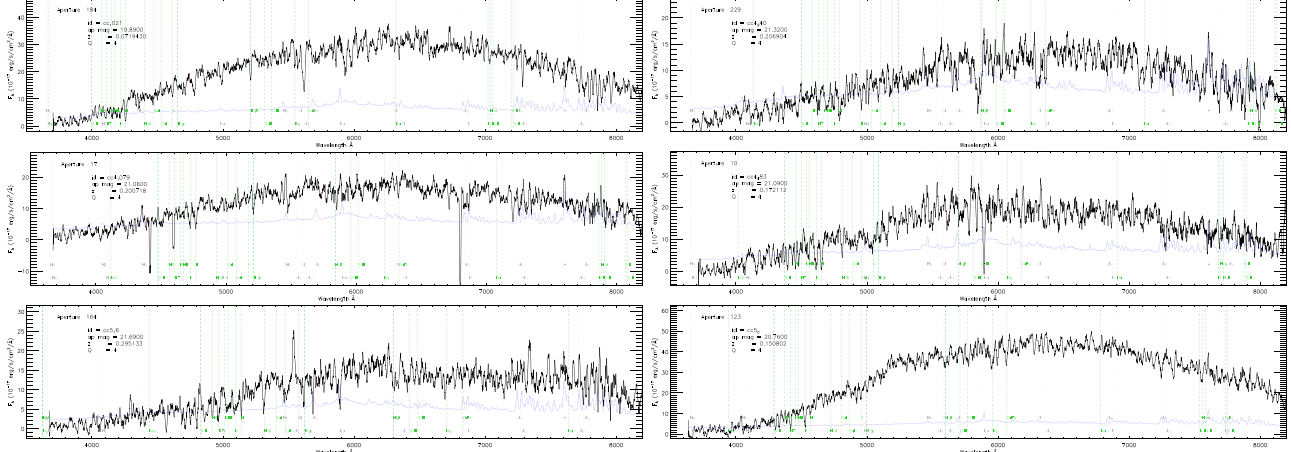


Figure 12. Example of spectra of low-mass galaxies ($10^9 M_\odot < M_* < 10^{9.5} M_\odot$) with weak emission lines.

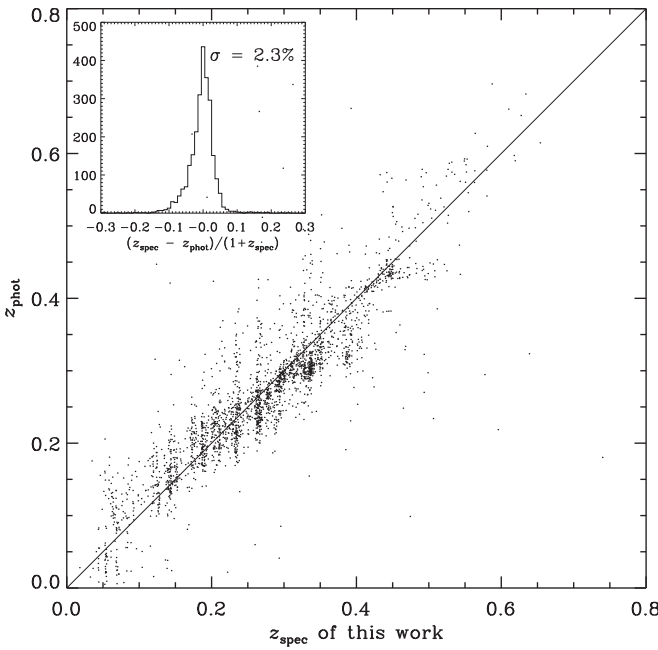


Figure 13. Our z_{spec} vs. the z_{phot} derived from the CLAUDS + HSC dr2 SEDs (G. Desprez et al. 2021, in preparation). The z_{phot} has a scatter about 2.3% and offset about 0.006. The large-scale clustering structures shown in z_{spec} are not recovered in the z_{phot} results.

We thank the referee for a careful reading and constructive suggestions. C.C. would like to thank Daniel Fabricant for approving the usage of MMT/Hectospec. We thank Zheng Cai,

Song Huang, and Cheng Li for helpful discussion. This work is supported by the National Key R&D Program of China grant 2017YFA0402704 and by the National Natural Science Foundation of China, Nos. 11803044, 11933003. This work is sponsored (in part) by the Chinese Academy of Sciences (CAS), through a grant to the CAS South America Center for Astronomy (CASSACA). We acknowledge the science research grants from the China Manned Space Project with No. CMS-CSST-2021-A05. This research uses data obtained through the Telescope Access Program (TAP). Observations reported here were obtained at the MMT Observatory, a joint facility of the University of Arizona and the Smithsonian Institution.

These data were obtained and processed as part of the CFHT Large Area *U*-band Deep Survey (CLAUDS), which is a collaboration between astronomers from Canada, France, and China described in Sawicki et al. (2019). CLAUDS is based on observations obtained with MegaPrime/MegaCam, a joint project of CFHT and CEA/DAPNIA, at the CFHT which is operated by the National Research Council (NRC) of Canada, the Institut National des Science de l’Univers of the Centre National de la Recherche Scientifique (CNRS) of France, and the University of Hawaii. CLAUDS uses data obtained in part through the Telescope Access Program (TAP), which has been funded by the National Astronomical Observatories, Chinese Academy of Sciences, and the Special Fund for Astronomy from the Ministry of Finance of China. CLAUDS uses data products from TERAPIX and the Canadian Astronomy Data Centre (CADC) and was carried out using resources from

Compute Canada and Canadian Advanced Network For Astrophysical Research (CANFAR).

This work is also based in part on data collected at the Subaru Telescope and retrieved from the HSC data archive system, which is operated by the Subaru Telescope and Astronomy Data Center at National Astronomical Observatory of Japan. The Hyper Suprime-Cam (HSC) collaboration includes the astronomical communities of Japan and Taiwan, and Princeton University. The HSC instrumentation and software were developed by the National Astronomical Observatory of Japan (NAOJ), the Kavli Institute for the Physics and Mathematics of the Universe (Kavli IPMU), the University of Tokyo, the High Energy Accelerator Research Organization (KEK), the Academia Sinica Institute for Astronomy and Astrophysics in Taiwan (ASIAA), and Princeton University. Funding was contributed by the FIRST program from Japanese Cabinet Office, the Ministry of Education, Culture, Sports, Science and Technology (MEXT), the Japan Society for the Promotion of Science (JSPS), Japan Science and Technology Agency (JST), the Toray Science Foundation, NAOJ, Kavli IPMU, KEK, ASIAA, and Princeton University.

Based on observations obtained with MegaPrime/Mega-Cam, a joint project of CFHT and CEA/IRFU, at the Canada–France–Hawaii Telescope (CFHT) which is operated by the National Research Council (NRC) of Canada, the Institut National des Sciences de l’Univers of the Centre National de la Recherche Scientifique (CNRS) of France, and the University of Hawaii. This work is based in part on data products produced at TERAPIX available at the Canadian Astronomy Data Centre as part of the Canada–France–Hawaii Telescope Legacy Survey, a collaborative project of NRC and CNRS.

ORCID iDs

- Cheng Cheng <https://orcid.org/0000-0003-0202-0534>
 Christopher N. A. Willmer <https://orcid.org/0000-0001-9262-9997>
 Hong-Xin Zhang <https://orcid.org/0000-0003-1632-2541>
 Matthew L. N. Ashby <https://orcid.org/0000-0002-3993-0745>
 Hai Xu <https://orcid.org/0000-0003-1094-5190>
 Marcin Sawicki <https://orcid.org/0000-0002-7712-7857>
 Stephen Gwyn <https://orcid.org/0000-0001-8221-8406>
 Guillaume Despres <https://orcid.org/0000-0001-8325-1742>
 Tianwen Cao <https://orcid.org/0000-0002-1335-6212>
 Gaoxiang Jin <https://orcid.org/0000-0003-3087-318X>
 Y. Sophia Dai <https://orcid.org/0000-0002-7928-416X>
 C. Kevin Xu <https://orcid.org/0000-0002-1588-6700>

References

- Aihara, H., AlSayyad, Y., Ando, M., et al. 2019, *PASJ*, **71**, 114
 Aihara, H., Arimoto, N., Armstrong, R., et al. 2018a, *PASJ*, **70**, S4
 Aihara, H., Armstrong, R., Bickerton, S., et al. 2018b, *PASJ*, **70**, S8
 Baldry, I. K., Glazebrook, K., Brinkmann, J., et al. 2004, *ApJ*, **600**, 681
 Baldwin, J. A., Phillips, M. M., & Terlevich, R. 1981, *PASP*, **93**, 5
 Balogh, M. L., Morris, S. L., Yee, H. K. C., Carlberg, R. G., & Ellingson, E. 1999, *ApJ*, **527**, 54
 Brown, T. M., Tumlinson, J., Geha, M., et al. 2014, *ApJ*, **796**, 91
 Bruzual, G., & Charlot, S. 2003, *MNRAS*, **344**, 1000
 Calzetti, D., Armus, L., Bohlin, R. C., et al. 2000, *ApJ*, **533**, 682
 Chabrier, G. 2003, *PASP*, **115**, 763
 Coil, A. L., Blanton, M. R., Burles, S. M., et al. 2011, *ApJ*, **741**, 8
 Coleman, G. D., Wu, C. C., & Weedman, D. W. 1980, *ApJS*, **43**, 393
 Cuillandre, J.-C. J., Withington, K., Hudelot, P., et al. 2012, *Proc. SPIE*, **8448**, 84480M
 Curti, M., Mannucci, F., Cresci, G., & Maiolino, R. 2020, *MNRAS*, **491**, 944
 Dahlen, T., Mobasher, B., Faber, S. M., et al. 2013, *ApJ*, **775**, 93
 Damjanov, I., Zahid, H. J., Geller, M. J., Fabricant, D. G., & Hwang, H. S. 2018, *ApJS*, **234**, 21
 Danieli, S., van Dokkum, P., & Conroy, C. 2018, *ApJ*, **856**, 69
 Dawson, K. S., Kneib, J.-P., Percival, W. J., et al. 2016, *AJ*, **151**, 44
 DESI Collaboration, Aghamousa, A., Aguilar, J., et al. 2016, arXiv:1611.00036
 Driver, S. P., Hill, D. T., Kelvin, L. S., et al. 2011, *MNRAS*, **413**, 971
 Driver, S. P., Wright, A. H., Andrews, S. K., et al. 2016, *MNRAS*, **455**, 3911
 Faber, S. M., Willmer, C. N. A., Wolf, C., et al. 2007, *ApJ*, **665**, 265
 Fabricant, D., Fata, R., Roll, J., et al. 2005, *PASP*, **117**, 1411
 Fang, J. J., Faber, S. M., Koo, D. C., et al. 2018, *ApJ*, **858**, 100
 Geach, J. E., Lin, Y. T., Makler, M., et al. 2017, *ApJS*, **231**, 7
 Geha, M., Blanton, M. R., Yan, R., & Tinker, J. L. 2012, *ApJ*, **757**, 85
 Geha, M., Wechsler, R. H., Mao, Y.-Y., et al. 2017, *ApJ*, **847**, 4
 González-Solares, E. A., Irwin, M., McMahon, R. G., et al. 2011, *MNRAS*, **416**, 927
 Grogin, N. A., Kocevski, D. D., Faber, S. M., et al. 2011, *ApJS*, **197**, 35
 Gunn, J. E., Siegmund, W. A., Mannery, E. J., et al. 2006, *AJ*, **131**, 2332
 Gwyn, S. D. J. 2012, *AJ*, **143**, 38
 Hill, G. J., Gebhardt, K., Komatsu, E., et al. 2008, in ASP Conf. Ser. 399, Panoramic Views of Galaxy Formation and Evolution, ed. T. Kodama, T. Yamada, & K. Aoki (San Francisco, CA: ASP), 115
 Hogg, D. W., Baldry, I. K., Blanton, M. R., & Eisenstein, D. J. 2002, arXiv: astro-ph/0210394
 Huang, J. S., Faber, S. M., Willmer, C. N. A., et al. 2013, *ApJ*, **766**, 21
 Ilbert, O., Salvato, M., Le Floc'h, E., et al. 2010, *ApJ*, **709**, 644
 Jarvis, M. J., Bonfield, D. G., Bruce, V. A., et al. 2013, *MNRAS*, **428**, 1281
 Jiang, L., Fan, X., Bian, F., et al. 2014, *ApJS*, **213**, 12
 Kauffmann, G., Heckman, T. M., Tremonti, C., et al. 2003, *MNRAS*, **346**, 1055
 Kewley, L. J., Dopita, M. A., Sutherland, R. S., Heisler, C. A., & Trevena, J. 2001, *ApJ*, **556**, 121
 Kewley, L. J., & Ellison, S. L. 2008, *ApJ*, **681**, 1183
 Kewley, L. J., Groves, B., Kauffmann, G., & Heckman, T. 2006, *MNRAS*, **372**, 961
 Kinney, A. L., Calzetti, D., Bohlin, R. C., et al. 1996, *ApJ*, **467**, 38
 Koekemoer, A. M., Faber, S. M., Ferguson, H. C., et al. 2011, *ApJS*, **197**, 36
 Kriek, M., van Dokkum, P. G., Labb  , I., et al. 2009, *ApJ*, **700**, 221
 Labb  , I., Huang, J., Franx, M., et al. 2005, *ApJL*, **624**, L81
 Lacy, M., Ridgway, S. E., Gates, E. L., et al. 2013, *ApJS*, **208**, 24
 Lawrence, A., Warren, S. J., Almaini, O., et al. 2007, *MNRAS*, **379**, 1599
 Le F  vre, O., Cassata, P., Cucciati, O., et al. 2013, *A&A*, **559**, A14
 Le F  vre, O., Tasca, L. A. M., Cassata, P., et al. 2015, *A&A*, **576**, A79
 Le F  vre, O., Vettolani, G., Garilli, B., et al. 2005, *A&A*, **439**, 845
 Leja, J., Tacchella, S., & Conroy, C. 2019, *ApJL*, **880**, L9
 Li, T. S., Koposov, S. E., Zucker, D. B., et al. 2019, *MNRAS*, **490**, 3508
 Lilly, S. J., Le Brun, V., Maier, C., et al. 2009, *ApJS*, **184**, 218
 Lilly, S. J., Le F  vre, O., Renzini, A., et al. 2007, *ApJS*, **172**, 70
 Liu, F. S., Jia, M., Yesuf, H. M., et al. 2018, *ApJ*, **860**, 60
 Lonsdale, C. J., Smith, H. E., Rowan-Robinson, M., et al. 2003, *PASP*, **115**, 897
 LSST Science Collaboration, Abell, P. A., Allison, J., et al. 2009, arXiv:0912.0201
 Ly, C., Malhotra, S., Malkan, M. A., et al. 2016a, *ApJS*, **226**, 5
 Ly, C., Malkan, M. A., Rigby, J. R., & Nagao, T. 2016b, *ApJ*, **828**, 67
 Mahajan, S., Drinkwater, M. J., Driver, S., et al. 2018, *MNRAS*, **475**, 788
 Maiolino, R., & Mannucci, F. 2019, *A&ARv*, **27**, 3
 Mao, Y.-Y., Geha, M., Wechsler, R. H., et al. 2021, *ApJ*, **907**, 85
 Mohammad, F. G., Bianchi, D., Percival, W. J., et al. 2018, *A&A*, **619**, A17
 Newman, J. A., Cooper, M. C., Davis, M., et al. 2013, *ApJS*, **208**, 5
 Nishizawa, A. J., Hsieh, B.-C., Tanaka, M., & Takata, T. 2020, arXiv:2003.01511
 Pan, Z., Zheng, X., Lin, W., et al. 2016, *ApJ*, **819**, 91
 Pierre, M., Chiappetti, L., Pacaud, F., et al. 2007, *MNRAS*, **382**, 279
 Roediger, J. C., Ferrarese, L., C  te, P., et al. 2017, *ApJ*, **836**, 120
 Roll, J. B., Fabricant, D. G., & McLeod, B. A. 1998, *Proc. SPIE*, **3355**, 324
 Rowan-Robinson, M., Gonzalez-Solares, E., Vaccari, M., & Marchetti, L. 2013, *MNRAS*, **428**, 1958
 Rowan-Robinson, M., Lari, C., Perez-Fournon, I., et al. 2004, *MNRAS*, **351**, 1290
 Salim, S. 2014, *SerAJ*, **189**, 1
 Salim, S., Charlot, S., Rich, R. M., et al. 2005, *ApJL*, **619**, L39

- Salvato, M., Ilbert, O., & Hoyle, B. 2019, *NatAs*, **3**, 212
- Sawicki, M., Arnouts, S., Huang, J., et al. 2019, *MNRAS*, **489**, 5202
- Schmidt, S. J., Malz, A. I., Soo, J. Y. H., et al. 2020, *MNRAS*, **499**, 1587
- Scoville, N., Aussel, H., Brusa, M., et al. 2007, *ApJS*, **172**, 1
- Shin, K., Ly, C., Malkan, M. A., et al. 2021, *MNRAS*, **501**, 2231
- Shirley, R., Duncan, K., Campos Varillas, M. C., et al. 2021, *MNRAS*, **507**, 129
- Simon, J. D. 2019, *ARA&A*, **57**, 375
- Sohn, J., Geller, M. J., Hwang, H. S., et al. 2021, *ApJ*, **909**, 129
- Strauss, M. A., Weinberg, D. H., Lupton, R. H., et al. 2002, *AJ*, **124**, 1810
- Takamiya, M., Kron, R. G., & Kron, G. E. 1995, *AJ*, **110**, 1083
- Tamura, N., Takato, N., Shimono, A., et al. 2016, *Proc. SPIE*, **9908**, 99081M
- Tanaka, M., Coupon, J., Hsieh, B.-C., et al. 2018, *PASJ*, **70**, S9
- Toloba, E., Guhathakurta, P., van de Ven, G., et al. 2014, *ApJ*, **783**, 120
- Tremonti, C. A., Heckman, T. M., Kauffmann, G., et al. 2004, *ApJ*, **613**, 898
- Wang, W., Faber, S. M., Liu, F. S., et al. 2017, *MNRAS*, **469**, 4063
- Williams, R. J., Quadri, R. F., Franx, M., et al. 2010, *ApJ*, **713**, 738
- Willmer, C. N. A., Faber, S. M., Koo, D. C., et al. 2006, *ApJ*, **647**, 853
- Wirth, G. D., Willmer, C. N. A., Amico, P., et al. 2004, *AJ*, **127**, 3121
- York, D. G., Adelman, J., Anderson, J. E., et al. 2000, *AJ*, **120**, 1579
- Zhou, R., Cooper, M. C., Newman, J. A., et al. 2019, *MNRAS*, **488**, 4565